Catalysis Science & Technology

ROYAL SOCIETY OF CHEMISTRY

PAPER

View Article Online
View Journal | View Issue

Check for updates

Cite this: *Catal. Sci. Technol.*, 2022, 12, 1922

Surface ligands enhance the catalytic activity of supported Au nanoparticles for the aerobic α-oxidation of amines to amides†

Puranjan Chatterjee, [ab] Hsin Wang, [ab] J. Sebastián Manzano, [ab] Uddhav Kanbur, [ab] Aaron D. Sadow [ab] and Igor I. Slowing *[ab]

Received 21st November 2021,
Accepted 3rd February 2022

DOI: 10.1039/d1cy02121d

rsc.li/catalysis

The catalytic aerobic α-oxidation of amines in water is an atom economic and green alternative to current methods of amide synthesis. The reaction uses O_2 as terminal oxidant, avoids hazardous reactants and gives water as the only byproduct. Here we report that the catalytic activity of silica-supported Au nanoparticles for the aerobic α-oxidation of amines can be improved by tethering pyridyl ligands to the support. In contrast, immobilization of thiol groups on the material gives activities comparable to Au supported on bare silica. Our studies indicate that the ligands affect the electronic properties of the Au nanoparticles and thereby determine their ability to activate O_2 and mediate C–H cleavage in the amine substrate. The reaction likely proceeds *via* an Au catalyzed β-hydride elimination enabled by backdonation from electron-rich metal to the σ^*_{C-H} orbital. O_2, which is also activated on electron-rich Au, acts as a scavenger to remove H from the metal surface and regenerate the active sites. The mechanistic understanding of the catalytic conversion led to a new approach for forming C–C bonds α to the N atoms of amines.

Introduction

Despite their wide application in high volume chemical commodities (*e.g.* plastics, antiblock agents, inks, pharmaceuticals, *etc.*)[1] amides are typically produced through methods that have poor atom economy, use hazardous reagents such as H_2SO_4, hydrazoic acid, acid chlorides, thionyl chloride, or produce large quantities of waste like SO_2, carboxylic acids or HCl.[2–8] Therefore, there has been great interest in developing more environmentally friendly and atom economic processes for their synthesis.[9,10]

The selective aerobic oxidation of amines is a promising approach to overcome these problems (eqn (1)).[11–14] This reaction is catalysed by Au powder in the presence of silica or by supported Au nanoparticles, and gives water as the only byproduct.[15–18] While supported Au nanoparticles (Au/CeO_2 and Au/Al_2O_3) have a broad substrate scope at low O_2 pressure, they have relatively low activity, with turnover numbers (TON) of *ca.* 25 for *N*-methylpyrrolidine over 24 h.[19,20] Besides, weak interactions of the metal with the supports result in Au sintering, which leads to a drop in its catalytic activity. Large Au particles are less active than their smaller counterparts because the latter have higher proportions of undercoordinated sites.[21–23] These sites are proposed to be the active centres in oxygen activation catalysis.[24,25] Therefore, preventing Au nanoparticle aggregation is necessary for attaining high catalytic activity. The sintering of metal nanoparticles depends on their chemical potential and adhesion energy to the support.[26,27] Modifying the surface of supports with organic ligands can enhance nanoparticle binding and decrease their chemical potential.[28–30] The interaction of nanoparticles with surface organic ligands raises the activation barriers for migration and thereby prevents sintering *via* Ostwald ripening.[31,32]

Importantly, surface-immobilized organic ligands can also affect the catalytic properties of supported nanoparticles in a similar way in which organic ligands control the reactivity of homogeneous catalysts *via* electronic or steric effects.[33–43] For instance, electron-donating ligands can increase the electron density of nanoparticles and modify their work function,[44] to ultimately affect their electrochemical potential in redox processes. Herein, we explored the effect of silica-grafted organic ligands on the selective aerobic oxidation of amines to amides catalysed by supported Au nanoparticles. We modified the surface of mesoporous silica nanoparticles (MSN) with thiol or pyridyl moieties, used them as supports for Au nanoparticles, and determined their catalytic performance in the aerobic oxidation of amines to amides.

[a] *U.S. Department of Energy, Ames Laboratory, Ames, Iowa 50011-3020, USA*
[b] *Department of Chemistry, Iowa State University, Ames, Iowa 50011-3111, USA. E-mail: islowing@iastate.edu*

† Electronic supplementary information (ESI) available. See DOI: 10.1039/d1cy02121d

We observed that while thiols provide strong interactions with the nanoparticles to prevent sintering, the supported Au has poor catalytic performance. In contrast, surface pyridyl species confer high activity (TON *ca.* 72 for *N*-methylpyrrolidine over 6 h) to the supported Au nanoparticles, while still averting sintering.

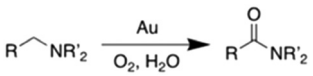

(1)

Experimental section

Materials

Hexadecyltrimethylammonium bromide, tetraethylorthosilicate, ethylene carbonate, deuterium oxide, *N*-methylpyrrolidine, *N*-methylpiperidine, pyrrolidine, piperidine, *N*,*N*-dimethylbutylamine, butylamine, *N*,*N*-diisopropyl ethylamine, 4-*tert*-butyl benzylamine, diethylamine phenylacetylene, 4-(*tert*-butyl)-benzyl bromide, and 5,5-dimethyl-1-pyrrolidine *N*-oxide (DMPO) were purchased from Sigma-Aldrich. 1-Benzylpyrrolidine was purchased from ChemScene. 2-(4-Pyridylethyl)triethoxysilane and 3-mercaptopropyl trimethoxysilane were purchased from Gelest, Inc. Gold(III) chloride was purchased from Alfa Aesar. Toluene and sodium hydroxide were purchased from Fisher. All reagents were used without further purification.

Specific surface area and porosimetry measurements

Textural properties of MSN, grafted MSNs and Au/R-MSNs were measured by nitrogen sorption isotherms at −196 °C in a Micromeritics Tristar Analyzer. The specific surface areas of the materials were calculated using the Brunauer–Emmett–Teller (BET) method and the pore widths with the Barrett–Joyner–Halenda (BJH) method. Pretreatment of the samples was done under N_2 flow at 100 °C for 6 h.

Elemental analysis

Organic group loadings were determined using a Perkin Elmer 2100 series II CHNS analyser. Acetanilide was used as a calibration standard with combustion and reduction temperatures 925 °C and 640 °C, respectively. All samples were prepared in triplicate.

Powder X-ray diffraction (XRD)

X-ray diffraction patterns of the materials were collected on a Bruker Siemens D500 X-ray diffractometer using Cu Kα radiation (40 kV, 44 mA) over the 0–10 and 30–70 2θ°. The samples were finely ground and compacted on top of a polycarbonate holder for obtaining the patterns.

Diffuse reflectance infrared Fourier transform spectroscopy (DRIFTS)

The infrared spectra of MSN, R-MSNs and Au/R-MSNs were collected on a Bruker Vertex 80 FT-IR spectrometer equipped with HeNe laser, photovoltaic MCT detector and OPUS software. A series of 64 scans with a resolution of 4 cm^{-1} were acquired to generate each spectrum in Kubelka–Munk mode. Samples were dried, finely ground and used neat for the measurements. For the high temperature experiments (100 °C), Au/PyEt-MSN (100 mg) was first impregnated with *N*-methylpyrrolidine (20 μL) and air-dried. The samples were then set in a Harrick Praying Mantis diffuse reflectance cell in a sealed ambient pressure chamber with ZnSe window. The spectra were collected every 5 min up to 30 min.

Inductively coupled plasma-optical emission spectroscopy (ICP-OES)

The Au loadings of Au/R-MSN were determined on a Perkin Elmer Optima 2100 DV inductively coupled plasma-optical emission spectroscope. The concentrations of Au were determined by interpolation in a calibration curve produced using freshly prepared standards. For the sample preparation, *ca.* 5 mg of Au/R-MSN were mixed with 0.2 mL HF solution (38–51%) in a 15 mL polypropylene centrifuge tube and vortexed overnight to dissolve the silica. 1.8 mL of freshly prepared aqua regia was added to this mixture and vortexed for 3 h at high speed. The samples were diluted with 10 mL DI H_2O (17.4 MΩ) and stirred for 1 h before analysing. Results are reported as an average of triplicates.

Pulse chemisorption

CO chemisorption was performed in a Micromeritics Autochem II Analyzer. *ca.* 100 mg of catalyst was placed in a U-tube sample holder and the following sequence was applied: the material was pretreated at 100 °C by flowing H_2 (10% in Ar) for 60 min to ensure the metal was fully reduced and then by flowing He for 60 min to remove excess surface bound H from the Au particles. The sample was then cooled to 80 °C under flowing He. The sample was then subjected to pulses of 10% CO in He. The % dispersion (D%) was of Au was determined as:

$$D\% = (S_f \times M \times V_{ad} \times 100)/(m \times W \times V_m)$$

where S_f = stoichiometry factor (Au/CO molar ratio) = 1, M = atomic mass of Au (196.97 g mol^{-1}), V_{ad} = volume of chemisorbed CO (mL) under standard temperature and pressure (STP) conditions, m = mass of sample (g), W = weight fraction of Au in the sample as determined from ICP-OES, and V_m = molar volume of CO (22 414 mL mol^{-1}) at STP.

Electron microscopy

Transmission electron microscopy (TEM) and high angle annular dark-field scanning transmission electron

microscopy (HAADF-STEM) were performed on a FEI Tecnai G2 F20 operating at 200 kV. The samples were prepared by placing 2–3 drops of dilute ethanol suspensions (*ca.* 0.1 mg mL^{-1}) of materials on a lacey-carbon-coated copper grid followed by air-drying.

Thermogravimetric analysis (TGA) and differential scanning calorimetry (DSC)

TGA–DSC was performed on Netzsch STA449 F1 instrument under air gas flow. The temperature was ramped at a rate of 10 K min^{-1} from 40 °C to 1000 °C. Approximately 9 mg of sample was placed in freshly cleaned alumina crucible for the run. The evolved gases were monitored by mass spectrometry using a range of m/z from 10 to 150. The data was analysed using Proteus software.

Nuclear magnetic resonance (NMR) spectroscopy

The ^{1}H NMR spectra of most products were collected in a Bruker Avance III 600 MHz instrument. ^{1}H NMR spectra of products **1** and **16** and ^{13}C NMR spectra of products **17**, **18**, **19**, **20** and **21** were collected in a Bruker Avance NEO 400 MHz instrument.

Electron paramagnetic resonance (EPR) spectroscopy

EPR spectra were collected on Bruker ELEXSYS E580 FT-EPR system. The spin trap DMPO (140.3 mg, 1.24 mmol) was dissolved in 1 mL toluene. 500 μL of this solution was mixed with the Au/PyEt-MSN or Au/MP-MSN catalysts (*ca.* 20 mg) exposed to air, and analysed by EPR. As controls, EPR spectra were collected for the original DMPO solution after exposure to air, and for a 500 μL aliquot of the DMPO solution mixed with *ca.* 20 mg Au/PyEt-MSN under N_2 inside a glovebox. The sample tube prepared in the glovebox was sealed under N_2 prior to taking it for EPR analysis.

Mass spectrometry

Mass spectra were collected on an Agilent QTOF 6540 MS using electrospray ionization in positive ion mode or on an Agilent GC–MS instrument (7890A, 5975C) equipped with HP-5MS column using electron impact ionization.

Mesoporous silica nanoparticle (MSN) synthesis

In a 5 L three-necked round bottom flask 5.10 g (14 mmol) of cetyltrimethylammonium bromide (CTAB) was dissolved in 2.4 L of deionized water. To this 17.5 mL of 2 M NaOH was added, and the reaction mixture was stirred at 550 rpm at 80 °C for 1 h. After this 25 mL (113 mmol) of tetraethylorthosilicate (TEOS) was added dropwise over a period of 10 min. The reaction mixture was further stirred for 2 h at 80 °C and 550 rpm. The product was then filtered and washed with abundant water and methanol and dried under vacuum at r.t. The dried product was then calcined at 550 °C for 6 h. BET surface area: 1320 m^2 g^{-1}, pore diameter: 2.6 nm, pore volume: 0.81 cm^3 g^{-1}. Powder XRD: (100) 2.46 2θ^o, (110) 4.23 2θ^o, (200) 4.89 2θ^o.

Grafting of MSN

In a typical procedure, 1.0 g of calcined MSN was suspended in 100 mL of toluene and then 3 mmol of organofunctional silane (2-(4-pyridylethyl)-triethoxysilane or 3-mercaptopropyl-trimethoxysilane) was added to the mixture. The mixture was then stirred at 500 rpm and heated at 100 °C for 12 h. The solid product was washed with water and methanol and dried under vacuum at r.t. overnight. The resulting products were designated PyEt-MSN and MP-MSN.

Catalyst preparation

2.85 μmol of $AuCl_3$ were dissolved in 50 mL of H_2O (0.06 mM). This solution was then added to 1 g of MSN, PyEt-MSN or MP-MSN in a 100 mL round bottom flask (target loading 0.5 wt%). The mixture was heated to 60 °C and stirred at 500 rpm for 1 h. The catalyst was then separated by filtration and washed thoroughly with water. After overnight drying under vacuum, the catalyst was reduced in a tube furnace under H_2 flow (15 mL min^{-1}) for 2 h at 100 °C. Catalysts with higher Au loading (4–5 wt% Au) were prepared by the same method but using 22.8 μmol of $AuCl_3$.

Catalytic α-oxidation of amines

A 10 mL Pyrex glass crimp tube was charged with 0.25 mol% of Au/R-MSN (*ca.* 50 mg catalyst with 0.5 wt% Au) followed by addition of 2 mL of DI H_2O. Then, 0.5 mmol of the amine was added, and the tube was plugged with a septum, crimped, and sealed. O_2 was flown through the overhead space of the solution for 3 min at 40 mL min^{-1} at r.t. The reaction mixture was then stirred at 1100 rpm and 100 °C for 6 h. The catalyst was separated by centrifugation, and the supernatant was diluted with D_2O and analysed by NMR using ethylene carbonate as internal standard. A 200 μL aliquot was drawn from the reaction mixture (2 mL) and combined with 400 μL D_2O and 100 μL of D_2O solution of ethylene carbonate standard (113 mM). The mixture was set in an NMR tube and the ^{1}H NMR was collected. Because of the basic conditions, a portion of ethylene carbonate is dissociated to ethylene glycol. The mmol of product were calculated using the following equation:

$$\text{mmol}P = \frac{I_\text{p}}{I_\text{EC} + I_\text{EG}} \times \frac{4}{H_\text{P}} \times \text{mmol EC} \times 10$$

where I_P is the integration of a reference peak in the product, I_EC the integration of the ethylene carbonate protons (4.5 ppm), I_EG the integration of the ethylene glycol protons (3.6 ppm), 4 is the number of protons in ethylene carbonate and ethylene glycol, H_P is the number of protons giving the reference product peak (*e.g.* for pyrrolidone Fig. S7,† the reference peak 1 at 3.35 ppm corresponds to 2 protons, so H_P is 2), mmol EC is the amount of ethylene carbonate standard

added to the mixture, and 10 is the ratio of aliquot to reaction mixture volumes. Sample spectra (please see below) are provided in Fig. S7.†

The turnover numbers (TON) for amide formation at any given time were calculated by dividing the mmoles of amide produced by the mmoles of Au used in the reaction (determined by ICP-OES).

Initial turnover frequencies (TOF_{ini}) for the catalytic α-oxidation of *N*-methylpyrrolidine

0.25 mol% Au/R-MSN (*ca.* 50 mg catalyst with 0.5 wt% Au) was added to a 10 mL Pyrex glass crimp tube, followed by addition of 2 mL of DI H_2O. 0.5 mmol (52 μL) of *N*-methylpyrrolidine was then added and the tube was plugged with a septum and crimped to seal. O_2 was flown through the overhead space of the solution for 3 min at 40 mL min^{-1} and r.t. The reaction mixture was then stirred at 1100 rpm and 85 °C for 0.5, 1, 1.5 or 2 h to obtain TON at different times. After each reaction time, the catalyst was separated from the solution by centrifugation, and the supernatant was diluted with D_2O and analysed by NMR using ethylene carbonate as internal standard.

The initial turnover frequencies (TOF_{ini}) were calculated as the slopes of the kinetic plots (time *vs.* TON).

Dehydrogenation of pyrrolidine to 5-(pyrrolidin-1-il)-3,4-dihydro-2*H*-pyrrole

0.25 mol% Au/PyEt-MSN (*ca.* 50 mg catalyst with 0.5 wt% Au) was added to a 10 mL Pyrex glass crimp tube followed by addition of 2 mL benzene. Then, 0.5 mmol (41 μL) of pyrrolidine was added, and the tube was crimped and sealed. O_2 was then flown through the overhead space of the solution for 3 min at 40 mL min^{-1} at r.t. The reaction mixture was then stirred at 1100 rpm and 100 °C for 6 h. The catalyst was separated by centrifugation, and the supernatant was diluted with $CDCl_3$ and analysed by NMR using ethylene carbonate as internal standard.

Conversion of imine to amide

The 5-(pyrrolidin-1-il)-3,4-dihydro-2*H*-pyrrole product was mixed with 2 mL of H_2O and heated at 100 °C for 6 h in presence of MSN (0.25 mol% Au). After catalyst centrifugation, the supernatant was diluted with D_2O and analysed by NMR using ethylene carbonate as internal standard.

Catalyst recycling

In a 10 mL Pyrex glass crimp tube 0.25 mol% Au/PyEt-MSN (*ca.* 50 mg catalyst with 0.5 wt% Au) was mixed with 2 mL DI H_2O and 0.5 mmol *N*-methylpyrrolidine. The tube was then sealed and O_2 was flown through the overhead space of the solution for 3 min at 40 mL min^{-1}. The mixture was then stirred at 1100 rpm for 2 h at 85 °C. After 2 h the reaction mixture was filtered while hot and the catalyst was washed with H_2O and acetone and dried under vacuum. The dried recovered catalyst was weighted and used for the subsequent runs. For each cycle the amount of amine used was adjusted so that the catalyst was 0.25 mol% of the amine. The volume of H_2O was also adjusted to make the concentration of amine 250 mM. Each cycle was done in duplicate. After the last run the material was analysed by ICP-OES to obtain the Au loading in the spent catalyst.

Synthesis of *N*,*N*-diethyl-4-(*tert*-butyl)-benzenemethanamine

0.6 mmol (110 μL) of 4-(*tert*-butyl)-benzyl bromide was mixed with 4 mL of toluene. 200 μL (1.1 mmol) of diisopropylethylamine and 0.72 mmol (76 μL) of diethylamine was added to the mixture. The reaction mixture was refluxed at 110 °C for 1 h. The reaction was quenched by the addition of H_2O, the product was extracted with EtOAc and concentrated under vacuum. The product was purified on a silica column using a hexanes : EtOAc = 60 : 1 mixture as mobile phase. The product was identified by NMR spectroscopy and used as a substrate for α-oxidation.

Coupling of amines with phenylacetylenes

A 10 mL Pyrex glass crimp tube was charged with 4 mol% Au/PyEt-MSN (*ca.* 100 mg of 4 wt% Au) catalyst and 2 mL (18 mmol) of phenylacetylene. 0.5 mmol of amine (*N*-methylpyrrolidine, *N*-methylpiperidine or *N*,*N*-diisopropylethylamine) was then added to the mixture. The system was sealed and O_2 was flown through the overhead space of the solution for 3 min at 40 mL min^{-1} at r.t. The reaction was stirred at 1100 rpm for 24 h at 100 °C. After the reaction, the catalyst was separated by centrifugation and the supernatant was concentrated under vacuum. The product was analysed by MS and NMR in $CDCl_3$ using ethylene carbonate as internal standard. For the substituted phenylacetylenes the reactions utilized 2 mL benzene as solvent and 5 mmol of the corresponding acetylene, all other conditions remained the same as those with phenylacetylene.

Results and discussion

Catalyst synthesis and characterization

To examine the effects of surface organic ligands on the behaviour of supported Au nanoparticle catalysts, we functionalized mesoporous silica nanoparticle (MSN) supports with groups containing thiol and pyridyl moieties (Scheme 1). Because of their strong interactions with

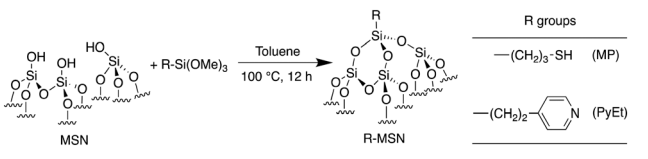

Scheme 1 Grafting of mesoporous silica nanoparticles (MSN) with mercaptopropyl- and 2-(4-pyridyl)ethyl-trimethoxysilanes to give MP-MSN and PyEt-MSN supports, respectively.

metals,[45–48] we expected –SH containing ligands would prevent Au nanoparticle aggregation.[20,49,50] The ligand was incorporated by grafting 3-mercaptopropyltrimethoxysilane onto the support, and the resulting material was designated as MP-MSN. Because recent reports have suggested that increasing the electron density in Au nanoparticles enhances catalytic activity for aerobic oxidations[51–53] we also selected pyridyl groups as surface ligands. We expected that their σ-donor character could give electron-enriched Au nanoparticles and thereby enhanced catalytic activity. To this end we grafted MSN with 2-(4-pyridyl)ethyltriethoxysilane and designated the resulting material as PyEt-MSN.

N_2 sorption and powder XRD analyses indicated that both MP-MSN and PyEt-MSN retained the high surface area and ordered hexagonal *p6mm* mesopore structure of the parent MSN material (Table S1, Fig. S1 and S2†). Elemental analyses confirmed presence of S and N in MP- and PyEt-MSN and provided estimates of group loadings at 1.42 ± 0.01 and 0.94 ± 0.01 mmol g^{-1}, respectively. DRIFTS analysis of the functionalized materials provided additional evidence of organic ligand incorporation. Specifically, the spectrum of MP-MSN showed characteristic bands of S–H (2582 cm^{-1}) and C–H (2900–2950 cm^{-1}) stretches (Fig. S3†), and PyEt-MSN (Fig. S4†) displayed bands corresponding to aliphatic and aromatic C–H stretches (2827–3080 cm^{-1}) and bends (1423–1456 cm^{-1}). In addition, PyEt-MSN had a band at 1612 cm^{-1} assigned to C═N stretch and a small absorption at 1562 cm^{-1} suggesting a fraction of the pyridyl groups were protonated *via* acid–base reaction with surface silanols.[54]

Au was then incorporated into the materials *via* deposition–precipitation from an aqueous $AuCl_3$ solution, followed by washing, drying and reduction of the powders at 100 °C under H_2 fow (Fig. S5, S6 and Table S2†). ICP-OES analysis indicated that both functionalized materials adsorbed and retained the target 0.5 wt% of the metal. In contrast, the non-functionalized parent MSN was only able to hold 0.03 wt% Au. Because the organic groups in MP-MSN and PyEt-MSN are present in a large excess relative to the Au, (mole ratios estimated at 55 : 1 and 35 : 1 for Au/MP-MSN and Au/PyEt-MSN, respectively), we deduce that the metal nanoparticles have a significantly stronger interaction with the grafted ligands in MP-MSN and PyEt-MSN than with the surface silanol or siloxy bridges of the original support. Due to the low metal loading, no significant differences were observed between the DRIFT spectra of Au/MP-MSN and that of the MP-MSN support. A slight variation with respect to the support was only observed in the spectrum of Au/PyEt-MSN (Fig. S8†), where a shoulder at 1635 cm^{-1} appeared next to the 1612 cm^{-1} C═N band, suggesting a fraction of the pyridyl groups were coordinating with the Au.[54,55] This shoulder became an actual peak for materials at higher Au loading (3.9 wt% Au). An additional peak was also observed at 1504 cm^{-1} in Au/PyEt-MSN further suggesting pyridyl–Au coordination.[56]

Thermogravimetric analysis (TGA) of the materials revealed that the organic functionalities were stable up to 200 °C (Fig. S9†). Small mass losses were observed for Au/MP-MSN (3.6 wt%) and Au/PyEt-MSN (2.3 wt%) below this temperature, and MS detection of the evolved gases indicated they corresponded to elimination of physisorbed water.

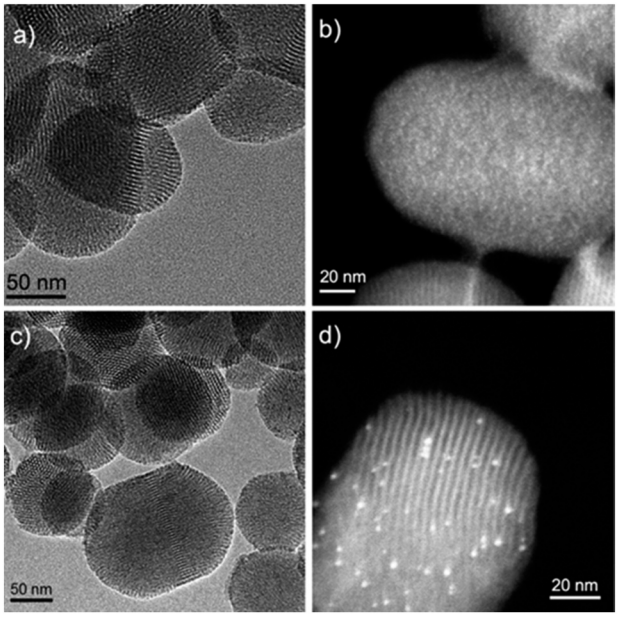

Fig. 1 Electron micrographs of Au/MP-MSN a) TEM and b) STEM, and Au/PyEt-MSN c) TEM and d) STEM.

Transmission electron microscopy (TEM) imaging of the materials (Fig. 1) revealed that the Au nanoparticles were smaller in Au/MP-MSN (<1 nm) than Au/PyEt-MSN (2.1 nm). The small particle sizes were consistent with high dispersions measured by CO pulsed chemisorption (52% and 44% for Au/MP-MSN and Au/PyEt-MSN, respectively) and with a lack of reflections corresponding to Au in the wide angle powder XRD patterns of the materials.[57,58] We note that while the Au nanoparticles in non-functionalized Au/MSN sintered within 10 s of exposure to the electron beam of the TEM (Fig. S10†), no changes were observed for Au/PyEt-MSN or Au/MP-MSN during image acquisition.

Effects of surface groups on catalytic activity

We then evaluated the activities of the materials as catalysts for the selective aerobic oxidation of *N*-methyl pyrrolidine to *N*-methyl pyrrolidone (0.25 M amine in water, 0.25 mol% Au, 3 min O_2 overhead flow, 85 °C). We calculated turnover numbers (TON) as mmoles of amide produced per mmol of Au in the catalyst. We derived initial turnover frequencies (TOF_{ini}) corresponding to initial rates from the slopes of the kinetic plots (time *vs.* TON, Fig. 2a). Interestingly, the activity of Au/PyEt-MSN (TOF: 10.2 h^{-1}) was almost the triple of that of Au/MP-MSN (TOF: 3.5 h^{-1}). We also tested the non-functionalized Au/MSN catalyst, which had a slightly better activity (TOF: 4.1 h^{-1}) than Au/MP-MSN. Importantly, neither Au/PyEt-MSN nor Au/MP-MSN gave any indications of particle sintering or Au loss even after prolonged reaction times (24 h, Fig. S11†). In contrast, no metal was detected by ICP-OES

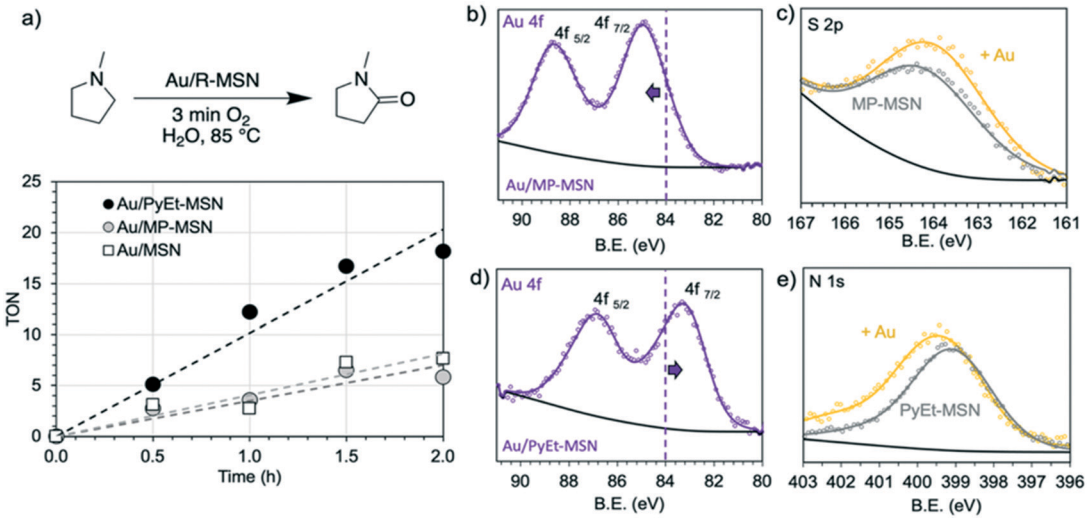

Fig. 2 a) Catalytic activities of Au/MP-MSN (grey circles), Au/PyEt-MSN (black circles) and Au/MSN (white squares) for the selective aerobic oxidation of *N*-methylpyrrolidine to *N*-methylpyrrolidone (conditions: 2 mL 0.25 M amine in H_2O, 0.25 mol% Au, 85 °C, 3 min O_2 overhead flow; TON = mmol of amide/mmol of Au). b) Au 4f and c) S 2p XP spectra of Au/MP-MSN, and d) Au 4f and e) N1s XP spectra of Au/PyEt-MSN. Discontinuous vertical line in b and d correspond to the position of the Au $4f_{7/2}$ peak in Au/MSN as a reference.

and TEM on the spent Au/MSN, indicating all Au leached out of the non-functionalized material.

Typically, activity decreases with increasing particle size.[59,60] Thus, the higher activity of the larger Au nanoparticles in Au/PyEt-MSN cannot be attributed to particle size effects. This idea was further supported by comparing the activity of the original Au/MP-MSN with a new Au/MP-MSN with larger Au nanoparticles (1.6 nm, Fig. S12†). The new material was prepared using a higher metal loading (4.8 wt%, Table S2†). As expected the new Au/MP-MSN with larger metal nanoparticles was even less active than the original Au/MP-MSN (2 h TON of 5.8 for the original catalyst and 1.4 for the material with 1.6 nm Au particles, Fig. S13†). Therefore, the lower TOF for amine oxidations catalyzed by Au/MP-MSN compared to Au/PyEt-MSN is not due to particle size. Instead, we propose that the differences are caused by changes in the electronic properties of Au induced by the surface ligands.

For completeness, we also prepared an Au/PyEt-MSN with higher metal loading (3.9 wt%) to obtain larger metal nanoparticles (3.2 nm) than the original Au/PyEt-MSN (Fig. S14 and Table S2†). Consistently, the Au/PyEt-MSN material with the larger metal particles gave a TON of 30 after 6 h compared to the TON of 66 over the same timespan provided by the original Au/PyEt-MSN with 2.1 nm particles (0.25 M amine in water, 0.25 mol% Au, 3 min O_2 overhead flow, 85 °C, Fig. S15†). We also note that increasing the PyEt– group loading from 1 to 1.4 mmol g^{-1} resulted in an increase in Au particle size to 2.5 nm, which led to a lower activity (TON of 44). In contrast, decreasing the PyEt– group loading to 0.64 mmol g^{-1} gave particles of similar size and the same catalytic activity as the original 0.94 mmol PyEt/g (Fig. S16†).

Recent reports have shown that increasing the electron density in Au benefits its catalytic activity for oxidation reactions.[61–63] For instance, the interaction of electron donating species with the surface of the metal can modify its work function and polarize the surface-solvent interface to facilitate O_2 activation.[53] Electron-rich Au surfaces activate adsorbed O_2 *via* backdonation from the metal d to the O π* orbital to produce surface-bound superoxo species.[61,64,65] We probed the electronic properties of the catalysts using XPS. The spectra revealed significant differences between the binding energies (BE) of their Au $4f_{7/2}$ electrons. While the Au $4f_{7/2}$ BE in Au/MP-MSN was higher than that of bulk Au^0 (85.0 *vs.* 83.9 eV (ref. 66)) the peak in Au/PyEt-MSN was shifted to a much lower value (83.1 eV) (Fig. 2b and d), suggesting that in spite of the reduction treatment (2 h under H_2 flow at 100 °C) Au had a cationic character in the former catalyst while the latter was electron-rich compared to the bulk metal. As a reference, the non-functionalized Au/MSN had an Au 4f BE centered at 83.9 eV, which is similar to that of bulk Au. These results indicate that surface ligands can control the electronic properties of the supported metal. We also observed small shifts in the S 2p and N 1s spectra of the ligands resulting from incorporation of Au into the supports. Importantly, these variations were complementary to the shifts observed in the corresponding Au $4f_{7/2}$ BE. For instance, the S 2p BE in Au/MP-MSN shifted to a slightly lower value (164.1 eV) than the original MP-MSN (164.2 eV, Fig. 2c). In contrast, the N 1s peak was slightly shifted towards higher BE (399.4 eV) compared to the parent PyEt-MSN (399.1 eV, Fig. 2e). Deconvolution of N 1s peak indicated that approximately 41% of the signal could be attributed to Au coordinated N (400.0 eV) (Fig. S17†).[67] Taken together, the negative and positive shifts in Au and N BE indicate that the PyEt group donates electrons to the metal. Therefore, the higher activity of Au/PyEt-MSN can be

attributed to electron donation of the ligand to the supported nanoparticles.

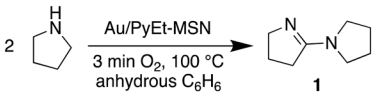

(2)

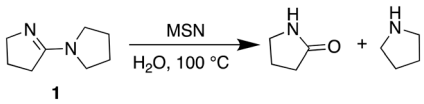

(3)

Reaction mechanism

Our experiments suggest that the Au/PyEt-MSN catalysed conversion of amine to amide utilizes O_2 as the terminal oxidant and water as oxygen donor. For instance, the Au/PyEt-MSN catalysed transformation of *N*-methyl pyrrolidine into *N*-methyl pyrrolidone gives a TON of 72 after 6 h under O_2 but only a TON of 2 under N_2 in the same timespan (0.25 M substrate in water, 0.25 mol% Au/PyEt-MSN, 100 °C, 3 min O_2 or N_2 overhead flow). While the Au/PyEt-MSN catalysed reaction of pyrrolidine under O_2 in water gives pyrrolidone (6 h TON: 17), no amide is formed in anhydrous benzene. The reaction product in absence of water is 5-(pyrrolidin-1-il)-3,4-dihydro-2*H*-pyrrole (**1**) (6 h TON: 19, eqn (2)). Yet dissolution of the isolated product **1** in water at the same reaction temperature in presence of MSN gave pyrrolidone (eqn (3)). The product **1**, however, resists hydrolysis to pyrrolidone in absence of MSN under the same conditions and reaction time, which indicates the silica support catalyses the hydrolysis step of the reaction (100 °C in water, 6 h reaction). Thus, the role of O_2 must be exclusively to assist the amine dehydrogenation, and does not participate in the formation of the new C=O bond. These results are consistent with previous reports of Au/Al_2O_3-catalysed amine oxidation using $^{18}O_2$ and $H_2{}^{18}O$ that showed the O in the amide product is provided by the water solvent rather than the O_2.[19]

While the reaction of pyrrolidine in anhydrous benzene gives product **1** and provides evidence for the formation of an imine intermediate, the tertiary amine *N*-methyl pyrrolidine does not give any product in absence of water. This lack of product formation cannot be attributed to low reactivity because *N*-methyl pyrrolidine is *ca.* 4 times more reactive than pyrrolidine in water under our reaction conditions (6 h TON: 72 *vs.* 17, respectively). Instead, the lack of product from the tertiary amine in benzene may be attributed to the reaction proceeding *via* an unstable iminium intermediate. Evidence for such intermediate is provided by DRIFTS analysis of Au/PyEt-MSN impregnated with *N*-methyl pyrrolidine. Heating the amine-impregnated catalyst in the DRIFTS cell to 100 °C results in the gradual emergence and growth of a band around 1578 cm^{-1}, which can be attributed to formation of an iminium on the surface of the material (Fig. 3a).[76–78] Co-impregnation of the material with the same substrate and water and heating to 100 °C results in the growth of a broad peak in the 1630 cm^{-1} to 1690 cm^{-1} region (Fig. 3b). As a reference, we collected the spectrum of *N*-methylpyrrolidone product adsorbed on the catalyst and observed two distinctive peaks centred at 1653 cm^{-1} and 1668 cm^{-1}. This suggests that the species formed in the co-impregnation experiment is indeed the reaction product. These results support the idea that the reaction may proceed through a β-hydride elimination, *i.e.* coordination of the amine N to Au followed by H abstraction to give the imine or iminium intermediate.

On the other hand, the adsorption of O_2 on electron-rich Au nanoparticles has been proposed to yield surface superoxo species.[61,65] This process involves electron transfer from Au to the adsorbed O_2 (O_2^*) and induces a decrease in the electron

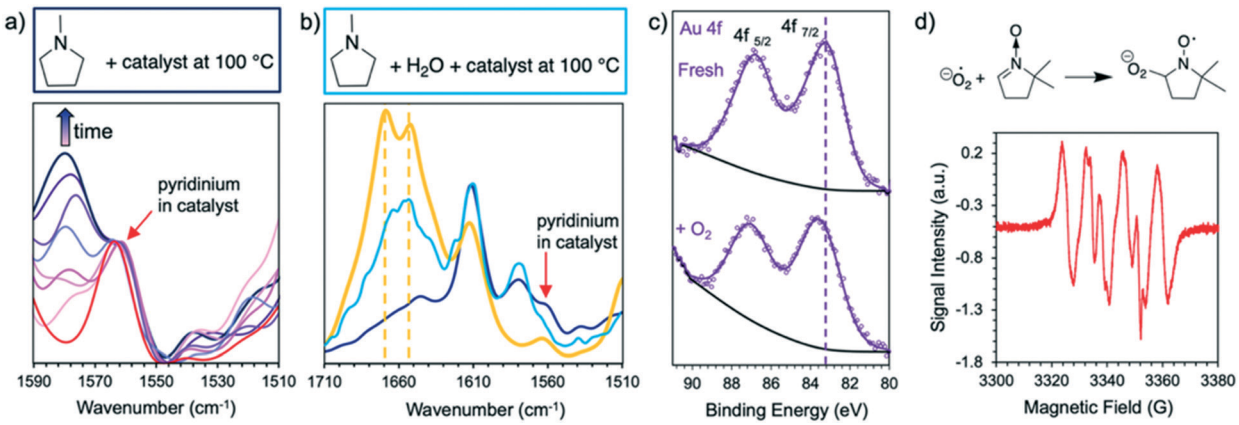

Fig. 3 a) DRIFT spectra of *N*-methyl pyrrolidone impregnated Au/PyEt-MSN at 100 °C collected every 5 min (pink to dark blue spectra) showing the emergence and growth of a band at 1578 cm^{-1} attributed to iminium. The red spectrum is the non-impregnated catalyst. b) DRIFT spectrum of *N*-methyl pyrrolidine and water co-impregnated Au/PyEt-MSN at 100 °C (light blue). The spectra of reaction product *N*-methyl pyrrolidone (yellow) and the last spectrum from a) (dark blue) provided as reference. c) Au 4f XP spectra of Au/PyEt-MSN catalyst before (top) and after (bottom) exposing to O_2. A 0.5 eV shift to higher binding energy is indicative of loss in electron density of the metal because of binding to O_2. d) EPR spectrum of Au/PyEt-MSN exposed to O_2 and treated with DMPO spin probe. The resulting spectrum is indicative of superoxide formation.

density of the metal.[68] Consistent with this information, XPS analysis of Au/PyEt-MSN catalyst treated with a stream of O_2 results in a 0.5 eV shift of the Au $4f_{7/2}$ peak to higher binding energy compared to the original catalyst (83.6 eV *vs.* 83.1 eV, respectively, Fig. 3c). This shift suggests binding of oxygen to the metal. The nature of surface oxygen species was investigated by reacting Au/PyEt-MSN exposed to air with 5,5′-dimethylpyrroline *N*-oxide (DMPO) spin trap. EPR spectroscopy analysis confirmed the formation of a nitroxyl adduct resulting from addition of superoxide species to DMPO (Fig. 3d).[69–71] Control experiments using 1) DMPO in air without catalyst gave only a weak signal, and 2) DMPO with the catalyst exposed to N_2 gave only noise in the EPR spectra (Fig. S18†). These results strongly suggest the formation of superoxide upon treating the catalyst with O_2. Furthermore, addition of superoxide quencher *p*-quinone[72–74] to the Au/PyEt-MSN catalysed reaction of *N*-methyl pyrrolidine also led to a drop in conversion (6 h TON of 20) under our standard conditions, further suggesting that these reactive oxygen species take part in the process.

We note that while the electron-deficient Au/MP-MSN is still able to mediate the reaction, its activity does not change upon flowing the system with N_2 instead of O_2 (6 h TON is 6 regardless of flowing with N_2 or O_2). Besides, addition of benzoquinone to the system does not alter the activity of Au/MP-MSN, and reaction with DMPO after O_2 treatment gives only background level EPR signal (Fig. S18d†). We also note that the Au/MP-MSN mediated reaction of *N*-methyl pyrrolidine reaches a maximum TON of 6 after 1.5 h and then the yield remains largely invariable at least until 6 h (in contrast, the same reaction catalysed by Au/PyEt-MSN gives a TON of 17 in 2 h that grows to 72 at 6 h). Thus, it appears that O_2 is not involved in the reaction in presence of the electron deficient Au/MP-MSN, and that O_2 does not participate in the early stages of the reaction catalysed by Au/PyEt-MSN. Instead, it is likely needed for catalyst turnover.

These results suggest that the catalytic process involves three fundamental components, specifically: the Au catalyst that mediates β-hydride elimination of the amine, water that provides O atoms for the amide product, and O_2 that enables the catalytic turnover. These components can be integrated into a possible catalytic cycle that involves an initial Au mediated β-hydride elimination along with amine deprotonation to give an imine (i), which then undergoes hydrolysis to give a carbinolamine (ii). A second β-hydride elimination and NH deprotonation of the intermediate leads to an iminol that tautomerizes to the amide (iii). Finally, reactive oxygen species formed in the electron-rich Au scavenge H from the nanoparticle surface along with the protons from steps i and iii to give water and allow catalyst turnover (iv) (Scheme 2). Thus, the H atoms in the water molecule that attacks the imine intermediate are eventually transferred to the reactive oxygen species to give new water molecules as a by product. Importantly, while β-hydride elimination is favoured by backdonation from electron-rich metal centres to the σ^*_{C-H} orbital, the process is less viable in electron poor Au.[75] Therefore, the difference in performance between Au/PyEt-MSN and Au/MP-MSN can be attributed to their opposing effects on the electronic properties of the Au nanoparticles. These differences in electronic properties control two critical steps of the catalytic cycle: C–H bond cleavage and O_2 activation. The more negative metal in Au/PyEt-MSN is more effective at inducing the cleavage of the C–H bond in the substrate to give an elimination product and activates O_2 to enable catalytic cycling. In contrast, the electron poor metal in Au/MP-MSN is unable to activate O_2 and behaves like a stoichiometric oxidant. We note that an additional effect of pyridyl moieties in Au/PyEt-MSN could be the promotion of nucleophilic water attack (step ii of the mechanism) by forming H-bonding interactions with water.

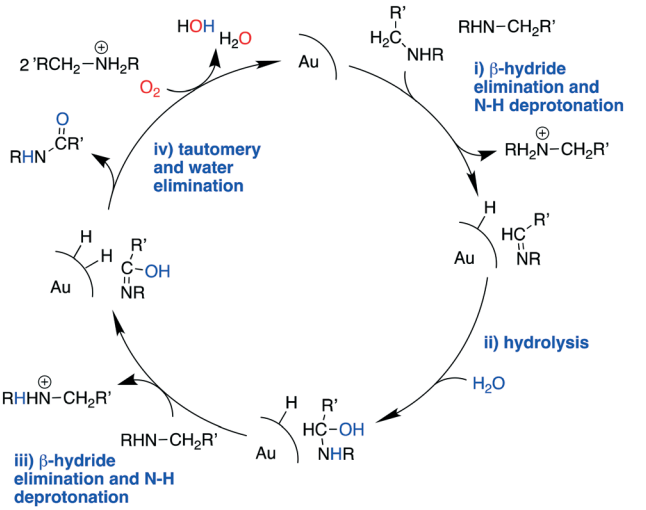

Scheme 2 Possible reaction mechanism for the Au/PyEt-MSN catalysed oxidation of amines to amides.

For completeness, we examined the recyclability of Au/PyEt-MSN. No significant drop in 2 h TON was observed over 5 recycling experiments (Fig. S19†). Furthermore, ICP-OES of the spent catalyst after the fifth cycle gave a 0.5 wt% Au indicating the pyridyl groups enabled retention of the metal, and XPS analysis of the spent catalyst indicated the metal remained electron rich (Au $4f_{7/2}$ peak centered at 83.5 eV compared to 83.9 eV of bulk Au) (Fig. S20†).

Effects of substrate structure on reactivity

The above results suggest that reaction rates should be favoured by the propensity of the substrates to undergo β-hydride elimination. Substrate structure-reactivity analysis indicates that catalytic rates are enhanced by increasing the degree of substitution of the amine (Table 1). The effect is likely due to electron donation by alkyl groups (*i.e.* inductive effect +*I*) that facilitates hydride formation. For example, under our standard conditions the reaction of the tertiary *N*,*N*-dimethyl butyl amine (**2**) gives a TON of 11 over 6 h, but no conversion is observed for the primary butyl amine (**3**) or the secondary diethyl amine (**4**) in the same timeframe (conditions: 100 °C, 0.25 mol% Au/PyEt-MSN, 3 min O_2 overhead flow). The

Table 1 Reactivity of amines as a function of their structure

Entry	Amine	Product	TON (6 h)
2			11
3		No reaction	N/A
4		No reaction	N/A
5			26
6			25
7			45
8			91
9		No reaction	N/A
10	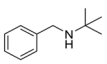	No reaction	N/A
11	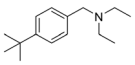	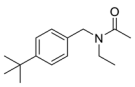	38
12	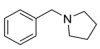	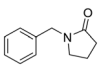	24
13			17
14			7
15			72
16			19

Reaction conditions: 0.5 mmol substrate, 0.25 mol% Au/PyEt-MSN (0.5 wt% Au), 2 mL H_2O, 100 °C, 6 h, 3 min O_2 overhead flow.

importance of electron donation by alkyl groups is further evidenced by the fact that the branched secondary *t*-butyl ethyl amine (**5**) is reactive (6 h TON of 26) but the linear secondary amine **4** is inert. Likewise, increasing the degree of α-alkyl substitution for tertiary amines leads to a consistent enhancement in reactivity: diethyl methyl amine (**6**) gives a TON of 25, triethyl amine (**7**) a TON of 45 and ethyl diisopropyl amine (**8**) reaches TON of 91 over the same reaction time and conditions as above. It is noteworthy that benzylamines do not react (*e.g.* benzylamine (**9**) or *t*-butyl benzylamine (**10**)), which suggests that the electron withdrawing inductive effect (*–I*) of aryl groups inhibits hydride elimination. An exception however, are tertiary dialkyl benzylamines like diethyl *p*-(*t*-butyl)benzyl amine (**11**) (TON of 38) or *N*-benzylpyrrolidine (**12**) (TON of 24). Importantly, the amides resulting from the reactions of amines **11** and **12** have the oxygen bound to the non-benzylic positions. These results further suggest that the electron-withdrawing inductive effect of aryl groups prevents hydride elimination (and therefore amide formation) at the benzylic position but the electron-donating effect of alkyl groups enables the loss of hydride on the aliphatic side of the molecules. Likewise, reactions of *N*-methylated amines show selective oxidation of the groups other than the methyl (*e.g.* butyl or ethyl in **2** and **6**, respectively). In contrast to the linear amines, cyclic secondary amines such as pyrrolidine (**13**) and piperidine (**14**) react well, the smaller cycle being more reactive than the latter (TON of 17 and 7, respectively). As expected, the corresponding *N*-methylated tertiary amines *N*-methylpyrrolidine (**15**) and *N*-methylpiperidine (**16**) are more reactive than the corresponding secondary amines, giving TON of 72 and 19, respectively. Overall, a clear trend is observed between the degree of alkyl substitution and the reactivity of the amine substrates. In contrast, the presence of additional functional groups with electron withdrawing inductive effect (*–I*) such as ether, alcohol, carboxylic acid, a second amine or bromine (Fig. S18†) inhibits the reaction. These results suggest that amine reactivity is favoured by the electron donation to the N atom.

Replacing water with acetylenes to form new C–C bonds

Finally, since the results above and proposed mechanism suggest that the O atom introduced at the α-carbon of the product results from the nucleophilic attack of H_2O, we considered that replacing water with another nucleophile could lead to other products. For example, as noted above, the reaction of pyrrolidine in absence of water gives an intermediate that is nucleophilically attacked by unreacted amine to give product **1** (eqn (2)). Therefore, we performed new reactions using neat phenylacetylene as reactant and solvent, with the expectation that deprotonated phenylacetylide could act as a nucleophile and attack the products of β-hydride elimination. Consistent with our hypothesis, we obtained 2-(phenylethynyl)-substituted amines **17–19** as products of the reactions of phenylacetylene with ethyl diisopropyl amine, *N*-methylpiperidine and

Table 2 Amine acetylene coupling reactions

Entry	Amine	Acetylene	Product	TON (24 h)
17			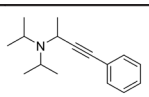	3[a]
18			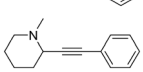	4[a]
19			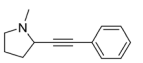	4[a]
20		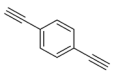	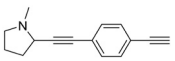	2[b]
21		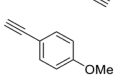		2[b]

[a] 0.5 mmol amine, 2 mL phenylacetylene, 4.0 mol% Au/PyEt-MSN (4.0 wt% Au), 3 min O_2 flow, 24 h at 100 °C. [b] 0.5 mmol amine, 2 mL benzene (solvent), 5.0 mmol substituted phenylacetylene, 4.0 mol% Au/PyEt-MSN (4.0 wt% Au), 3 min O2 flow, 24 h at 100 °C.

N-methylpyrrolidine, respectively (Table 2, 4 mol% Au/PyEt-MSN, 100 °C, 24 h). We note that this reaction utilizes an excess of the alkyne, therefore, when attempting the conversion of *N*-methylpyrrolidine with 1,4-diethynyl benzene only the 1 : 1 coupling product **20** was obtained. Increasing the concentration of the amine inhibits the reaction. The conversion does not proceed with linear terminal alkynes such as 1-octyne under our conditions. Using p-MeO substituted phenylacetylene as reactant gives the coupling product **21**, but p-CN and p-NH_2 substituted phenylacetylenes give no conversion. A possible reason for the lack of reactivity of the latter is the propensity of nitrile and amine groups to bind to Au, which may decrease the number of sites available for *N*-methylpyrrolidine activation. This reaction provides a new approach for C–C bond formation at position α to amines, and we plan to further explore and develop it. To the best of our knowledge, this transformation has only been attained with organometallic reagents,[79–82] therefore this is likely the first report of a heterogeneous catalyst giving this type of amine–alkyne coupling reaction.

Conclusions

In summary, organic ligands immobilized on a silica surface affect the electronic properties of supported Au nanoparticles. The effects of ligands are revealed by shifts in the X-ray photoelectron spectra of the metal. Thiol and pyridyl groups make the metal less and more electron-rich compared to Au on the non-modified support, respectively. These variations in electron density affect the catalytic performance of the metal in the aerobic oxidation of amines. Specifically, the electron-rich metal in Au/PyEt-MSN can backdonate electrons to the σ^*_{C-H} orbital in the substrate to induce C–H bond cleavage, while the electron-poor Au/MP-MSN has a more limited backdonation capacity. Furthermore, O_2 is activated on the electron-rich Au/PyEt-MSN as a superoxide, which allows sustaining the catalytic cycle by removal of chemisorbed hydrides from the metal surface. In contrast, the electron poor thiol-ligated Au does not seem to interact with O_2 and behaves as a stoichiometric oxidant rather than as a catalyst. Following the initial Au-catalysed β-hydride elimination, the intermediate imine undergoes a nucleophilic attack by water. A second β-hydride elimination followed by tautomerization yields the final amide. Based on this mechanism it is possible to introduce other groups on the α-carbon of amines by merely replacing water with a different nucleophile. An example of this is the reaction of phenylacetylene with amines, which in presence of Au/PyEt-MSN catalyst and O_2 yields α-substituted alkynylamines. Overall, this is work demonstrates a green and atom-economic approach to transform amines into amides or α-substituted amines.

Conflicts of interest

There are no conflicts to declare.

Acknowledgements

This research was supported by the U.S. Department of Energy, Office of Basic Energy Sciences, Division of Chemical Sciences, Geosciences, and Biosciences, through the Ames Laboratory Catalysis Science program. The Ames Laboratory is operated for the U.S. Department of Energy by Iowa State University under Contract No. DE-AC02-07CH11358.

Notes and references

1 J. Kroschwitz, *Kirk-Othmer Encyclopedia of Chemical Technology*, Wiley, New York, 4th edn, 1991.
2 A. H. Blatt, *Chem. Rev.*, 1933, **12**, 215–260.
3 K. F. Schmidt, *Ber. Dtsch. Chem. Ges. A*, 1924, **57**(4), 704–706.
4 N. O. V. Sonntag, *Chem. Rev.*, 1953, **52**, 237–416.
5 A. Leggio, E. L. Belsito, G. De Luca, M. L. Di Gioia, V. Leotta, E. Romio, C. Siciliano and A. Liguori, *RSC Adv.*, 2016, **6**, 34468–34475.
6 B. Thern, J. Rudolph and G. Jung, *Tetrahedron Lett.*, 2002, **43**, 5013–5016.
7 E. Valeur and M. Bradley, *Chem. Soc. Rev.*, 2009, **38**, 606–631.
8 E. K. Nelson, *J. Am. Chem. Soc.*, 1919, **41**, 2121–2130.
9 D. J. C. Constable, P. J. Dunn, J. D. Hayler, G. R. Humphrey, J. J. L. Leazer, R. J. Linderman, K. Lorenz, J. Manley, B. A. Pearlman, A. Wells, A. Zaks and T. Y. Zhang, *Green Chem.*, 2007, **9**, 411–420.
10 M. C. Bryan, P. J. Dunn, D. Entwistle, F. Gallou, S. G. Koenig, J. D. Hayler, M. R. Hickey, S. Hughes, M. E. Kopach, G. Moine, P. Richardson, F. Roschangar, A. Steven and F. J. Weiberth, *Green Chem.*, 2018, **20**, 5082–5103.
11 W. Xu, Y. Jiang and H. Fu, *Synlett*, 2012, **23**, 801–804.
12 J. R. Khusnutdinova, Y. Ben-David and D. Milstein, *J. Am. Chem. Soc.*, 2014, **136**, 2998–3001.
13 J. W. Kim, K. Yamaguchi and N. Mizuno, *Angew. Chem., Int. Ed.*, 2008, **47**, 9249–9251.
14 Y. Wang, H. Kobayashi, K. Yamaguchi and N. Mizuno, *Chem. Commun.*, 2012, **48**, 2642–2644.
15 B. Zhu and R. J. Angelici, *Chem. Commun.*, 2007, 2157–2159.
16 L. Aschwanden, T. Mallat, F. Krumeich and A. Baiker, *J. Mol. Catal. A: Chem.*, 2009, **309**, 57–62.
17 B. Zhu, M. Lazar, B. G. Trewyn and R. J. Angelici, *J. Catal.*, 2008, **260**, 1–6.
18 H. Chen, C. Liu, M. Wang, C. Zhang, N. Luo, Y. Wang, H. Abroshan, G. Li and F. Wang, *ACS Catal.*, 2017, **7**, 3632–3638.
19 X. Jin, K. Kataoka, T. Yatabe, K. Yamaguchi and N. Mizuno, *Angew. Chem., Int. Ed.*, 2016, **55**, 7212–7217.
20 T. O. Dairo, N. C. Nelson, I. I. Slowing, R. J. Angelici and L. K. Woo, *Catal. Lett.*, 2016, **146**, 2278–2291.
21 H. Tsunoyama, H. Sakurai and T. Tsukuda, *Chem. Phys. Lett.*, 2006, **429**, 528–532.
22 D. V. Jawale, E. Gravel, V. Geertsen, H. Li, N. Shah, R. Kumar, J. John, I. N. N. Namboothiri and E. Doris, *Tetrahedron*, 2014, **70**, 6140–6145.

23 T. V. W. Janssens, B. S. Clausen, B. Hvolbæk, H. Falsig, C. H. Christensen, T. Bligaard and J. K. Nørskov, *Top. Catal.*, 2007, **44**, 15.
24 D. C. Lim, I. Lopez-Salido, R. Dietsche, M. Bubek and Y. D. Kim, *Chem. Phys.*, 2006, **330**, 441–448.
25 M. Turner, V. B. Golovko, O. P. H. Vaughan, P. Abdulkin, A. Berenguer-Murcia, M. S. Tikhov, B. F. G. Johnson and R. M. Lambert, *Nature*, 2008, **454**, 981–983.
26 Y. Dai, P. Lu, Z. Cao, C. T. Campbell and Y. Xia, *Chem. Soc. Rev.*, 2018, **47**, 4314–4331.
27 J. A. Farmer and C. T. Campbell, *Science*, 2010, **329**, 933.
28 S. Rana, S. Maddila, K. Yalagala and S. B. Jonnalagadda, *Appl. Catal., A*, 2015, **505**, 539–547.
29 J. S. Manzano, H. Wang, T. Kobayashi, P. Naik, K. C. Lai, J. W. Evans and I. I. Slowing, *Microporous Mesoporous Mater.*, 2020, 110276.
30 C. M. Crudden, M. Sateesh and R. Lewis, *J. Am. Chem. Soc.*, 2005, **127**, 10045–10050.
31 L. Xin, F. Yang, S. Rasouli, Y. Qiu, Z.-F. Li, A. Uzunoglu, C.-J. Sun, Y. Liu, P. Ferreira, W. Li, Y. Ren, L. A. Stanciu and J. Xie, *ACS Catal.*, 2016, **6**, 2642–2653.
32 R. van den Berg, T. E. Parmentier, C. F. Elkjær, C. J. Gommes, J. Sehested, S. Helveg, P. E. de Jongh and K. P. de Jong, *ACS Catal.*, 2015, **5**, 4439–4448.
33 C. Parise, B. Ballarin, D. Barreca, M. C. Cassani, P. Dambruoso, D. Nanni, I. Ragazzini and E. Boanini, *Appl. Surf. Sci.*, 2019, **492**, 45–54.
34 P. Wu, P. Bai, Z. Lei, K. P. Loh and X. S. Zhao, *Microporous Mesoporous Mater.*, 2011, **141**, 222–230.
35 P. Wu, P. Bai, K. P. Loh and X. S. Zhao, *Catal. Today*, 2010, **158**, 220–227.
36 Z. Cao, J. S. Derrick, J. Xu, R. Gao, M. Gong, E. M. Nichols, P. T. Smith, X. Liu, X. Wen, C. Copéret and C. J. Chang, *Angew. Chem., Int. Ed.*, 2018, **57**, 4981–4985.
37 Y. Chen, Z. Guo, T. Chen and Y. Yang, *J. Catal.*, 2010, **275**, 11–24.
38 G. Chen, C. Xu, X. Huang, J. Ye, L. Gu, G. Li, Z. Tang, B. Wu, H. Yang, Z. Zhao, Z. Zhou, G. Fu and N. Zheng, *Nat. Mater.*, 2016, **15**, 564–569.
39 S. Kunz, *Top. Catal.*, 2016, **59**, 1671–1685.
40 K. Mori, S. Masuda, H. Tanaka, K. Yoshizawa, M. Che and H. Yamashita, *Chem. Commun.*, 2017, **53**, 4677–4680.
41 X.-K. Wan, J.-Q. Wang, Z.-A. Nan and Q.-M. Wang, *Sci. Adv.*, 2017, **3**, e1701823.
42 N. Ishito, K. Nakajima, Y. Maegawa, S. Inagaki and A. Fukuoka, *Catal. Today*, 2017, **298**, 258–262.
43 L. Lu, S. Zou and B. Fang, *ACS Catal.*, 2021, **11**, 6020–6058.
44 P. Wang, D. Tanaka, S. Ryuzaki, S. Araki, K. Okamoto and K. Tamada, *Appl. Phys. Lett.*, 2015, **107**, 151601.
45 A. I. Frenkel, S. Nemzer, I. Pister, L. Soussan, T. Harris, Y. Sun and M. H. Rafailovich, *J. Chem. Phys.*, 2005, **123**, 184701.
46 M. K. Corbierre and R. B. Lennox, *Chem. Mater.*, 2005, **17**, 5691–5696.
47 C. K. Yee, R. Jordan, A. Ulman, H. White, A. King, M. Rafailovich and J. Sokolov, *Langmuir*, 1999, **15**, 3486–3491.
48 G. H. Woehrle, L. O. Brown and J. E. Hutchison, *J. Am. Chem. Soc.*, 2005, **127**, 2172–2183.
49 T. V. Choudhary and D. W. Goodman, *Top. Catal.*, 2002, **21**, 25–34.
50 J. P. Gabaldon, M. Bore and A. K. Datye, *Top. Catal.*, 2007, **44**, 253–262.
51 M. Okumura, Y. Kitagawa, M. Haruta and K. Yamaguchi, *Chem. Phys. Lett.*, 2001, **346**, 163–168.
52 S. Karanjit, K. Bobuatong, R. Fukuda, M. Ehara and H. Sakurai, *Int. J. Quantum Chem.*, 2013, **113**, 428–436.
53 Q. Gu, P. Sautet and C. Michel, *ACS Catal.*, 2018, **8**, 11716–11721.
54 M. I. Zaki, M. A. Hasan, F. A. Al-Sagheer and L. Pasupulety, *Colloids Surf., A*, 2001, **190**, 261–274.
55 Q. Zhang, H. Su, J. Luo and Y. Wei, *Tetrahedron*, 2013, **69**, 447–454.
56 S. Muratsugu, M. H. Lim, T. Itoh, W. Thumrongpatanaraks, M. Kondo, S. Masaoka, T. S. Andy Hor and M. Tada, *Dalton Trans.*, 2013, **42**, 12611–12619.
57 Y. Liu, H. Tsunoyama, T. Akita, S. Xie and T. Tsukuda, *ACS Catal.*, 2011, **1**, 2–6.
58 Y. Kotolevich, O. Martynyuk, S. Martínez-González, H. Tiznado, A. Pestryakov, M. Avalos Borja, V. Cortés Corberán and N. Bogdanchikova, *Fuel*, 2019, **236**, 589–597.
59 H. Tsunoyama, H. Sakurai, Y. Negishi and T. Tsukuda, *J. Am. Chem. Soc.*, 2005, **127**, 9374–9375.
60 L. Alves, B. Ballesteros, M. Boronat, J. R. Cabrero-Antonino, P. Concepción, A. Corma, M. A. Correa-Duarte and E. Mendoza, *J. Am. Chem. Soc.*, 2011, **133**, 10251–10261.
61 F. Wang, W. Ueda and J. Xu, *Angew. Chem., Int. Ed.*, 2012, **51**, 3883–3887.
62 S. Nishimura, Y. Yakita, M. Katayama, K. Higashimine and K. Ebitani, *Catal. Sci. Technol.*, 2013, **3**, 351–359.
63 M. L. Kimble, A. W. Castleman, R. Mitrić, C. Bürgel and V. Bonačić-Koutecký, *J. Am. Chem. Soc.*, 2004, **126**, 2526–2535.
64 A. Staykov, T. Nishimi, K. Yoshizawa and T. Ishihara, *J. Phys. Chem. C*, 2012, **116**, 15992–16000.
65 H. Tsunoyama, N. Ichikuni, H. Sakurai and T. Tsukuda, *J. Am. Chem. Soc.*, 2009, **131**, 7086–7093.
66 A. Y. Klyushin, T. C. R. Rocha, M. Hävecker, A. Knop-Gericke and R. Schlögl, *Phys. Chem. Chem. Phys.*, 2014, **16**, 7881–7886.
67 R. J. J. Jansen and H. van Bekkum, *Carbon*, 1995, **33**, 1021–1027.
68 S. Laursen and S. Linic, *Phys. Rev. Lett.*, 2006, **97**, 026101.
69 F. Su, S. C. Mathew, G. Lipner, X. Fu, M. Antonietti, S. Blechert and X. Wang, *J. Am. Chem. Soc.*, 2010, **132**, 16299–16301.
70 M. Yamada, K. D. Karlin and S. Fukuzumi, *Chem. Sci.*, 2016, **7**, 2856–2863.
71 X.-Q. Deng, B. Zhu, X.-S. Li, J.-L. Liu, X. Zhu and A.-M. Zhu, *Appl. Catal., B*, 2016, **188**, 48–55.
72 M.-T. Maurette, E. Oliveros, P. P. Infelta, K. Ramsteiner and A. M. Braun, *Helv. Chim. Acta*, 1983, **66**, 722–733.
73 E. Lee-Ruff, *Chem. Soc. Rev.*, 1977, **6**, 195–214.
74 O. Fónagy, E. Szabó-Bárdos and O. Horváth, *J. Photochem. Photobiol., A*, 2021, **407**, 113057.

75 F. Rekhroukh, L. Estevez, S. Mallet-Ladeira, K. Miqueu, A. Amgoune and D. Bourissou, *J. Am. Chem. Soc.*, 2016, **138**, 11920–11929.
76 A. Comas-Vives, C. González-Arellano, A. Corma, M. Iglesias, F. Sánchez and G. Ujaque, *J. Am. Chem. Soc.*, 2006, **128**, 4756–4765.
77 K. M. Parida, S. Singha, P. C. Sahoo and S. Sahu, *J. Mol. Catal. A: Chem.*, 2011, **342–343**, 11–17.
78 G. R. Reddy, S. Balasubramanian and K. Chennakesavulu, *J. Mater. Chem. A*, 2014, **2**, 15598–15610.
79 M. Yamaguchi and I. Hirao, *Tetrahedron Lett.*, 1983, **24**, 1719–1722.
80 T. Murai, R. Toshio and Y. Mutoh, *Tetrahedron*, 2006, **62**, 6312–6320.
81 A. Paul and D. Seidel, *J. Am. Chem. Soc.*, 2019, **141**, 8778–8782.
82 Y. Cui, W. Lin and S. Ma, *Chem. Sci.*, 2019, **10**, 1796–1801.